The Journal of Chemical Physics ARTICLE scitation.org/journal/jcp

Tuning interfacial charge transfer in atomically precise nanographene–graphene heterostructures by engineering van der Waals interactions

Cite as: J. Chem. Phys. 156, 074702 (2022); doi: 10.1063/5.0081074
Submitted: 6 December 2021 • Accepted: 27 January 2022 •
Published Online: 15 February 2022

View Online Export Citation CrossMark

Xiaoqing Yu,[1] Shuai Fu,[1] Mukunda Mandal,[1] Xuelin Yao,[1] Zhaoyang Liu,[2] Wenhao Zheng,[1] Paolo Samorì,[2] Akimitsu Narita,[1,3] Klaus Müllen,[1] Denis Andrienko,[1] Mischa Bonn,[1] and Hai I. Wang[1,a)]

AFFILIATIONS

[1] Max Planck Institute for Polymer Research, Ackermannweg 10, 55128 Mainz, Germany
[2] CNRS, ISIS UMR 7006, University of Strasbourg, 8 allée Gaspard Monge, 67000 Strasbourg, France
[3] Organic and Carbon Nanomaterials Unit, Okinawa Institute of Science and Technology Graduate University, Okinawa, Japan

Note: This paper is part of the JCP Special Topic on Transport of Charge and Energy in Low-Dimensional Materials.
[a)] **Author to whom correspondence should be addressed:** wanghai@mpip-mainz.mpg.de

ABSTRACT

Combining strong light absorption and outstanding electrical conductivity, hybrid nanographene–graphene (NG–Gr) van der Waals heterostructures (vdWHs) represent an emerging material platform for versatile optoelectronic devices. Interfacial charge transfer (CT), a fundamental process whose full control remains limited, plays a paramount role in determining the final device performance. Here, we demonstrate that the interlayer vdW interactions can be engineered by tuning the sizes of bottom-up synthesized NGs to control the interfacial electronic coupling strength and, thus, the CT process in NG–Gr vdWHs. By increasing the dimensions of NGs from 42 to 96 sp^2 carbon atoms in the polyaromatic core to enhance the interfacial coupling strength, we find that the CT efficiency and rate in NG–Gr vdWHs display a drastic increase of one order of magnitude, despite the fact that the interfacial energy driving the CT process is unfavorably reduced. Our results shed light on the CT mechanism and provide an effective knob to tune the electronic coupling at NG–Gr interfaces by controlling the size-dependent vdW interactions.

© 2022 Author(s). All article content, except where otherwise noted, is licensed under a Creative Commons Attribution (CC BY) license (http://creativecommons.org/licenses/by/4.0/). https://doi.org/10.1063/5.0081074

I. INTRODUCTION

Nanographenes (NGs) are a group of extended polyaromatic hydrocarbons with a lateral size larger than 1 nm, which possess fascinating electronic and optical properties, including tunable and strong optical absorption, high photoluminescence (PL) quantum yields, and stimulated emission.[1–6] Integration of NGs with graphene (Gr) constitutes hybrid van der Waals heterostructures (vdWHs) combining strong light–matter interaction with outstanding electrical conductivity. As such, these vdWHs provide a novel platform for exploiting intriguing optoelectronic phenomena and developing versatile devices. For instance, Yan *et al.*[7] employed vdWHs composed of exfoliated Gr and NGs as the bifunctional electrodes for photoelectrochemical water splitting, simultaneously achieving efficient oxygen and hydrogen evolution. Furthermore, Liu *et al.*[8] sensitized Gr by solution-processed NGs toward highly efficient photodetection.[9] The large interfacial electronic coupling caused by the strong π–π interaction at the NG–Gr interface drives the transfer of the photogenerated holes from NGs to Gr with high efficiency (~10%). Moreover, the charge separation time was found to be extremely long (over 1 ns), enabling effective photogating in Gr. These two fascinating charge transfer (CT) characteristics enable high-performance photodetectors with an ultrahigh responsivity up to 4.5×10^7 A/W and a specific detectivity of 4.6×10^{13} Jones, being competitive with the state-of-the-art Gr-based heterostructures.[10–14] In the heart of these applications, interfacial CT plays a critical role in determining the final performance, yet has remained largely uncontrollable.

© Author(s) 2022

Recent advances in the bottom-up synthesis of NGs enable atomically precise tuning of their geometries, edge structures, and lateral sizes,[15–20] offering a potential approach to boost the CT efficiency by regulating the interaction between the adjacent layers and engineering the band alignment at the interface. For example, NGs with larger lateral sizes are expected to adhere much stronger to Gr,[21,22] thanks to the enhanced interfacial vdW interactions [as shown in Fig. 1(a)], even when normalized to the number of carbon atoms.[22] This could increase electronic coupling at NG–Gr interfaces, thus facilitating CT. On the other hand, the driving force ($-\Delta G$) for CT, i.e., the energy difference between the highest occupied molecular orbital (HOMO) in NGs and the Fermi level in Gr (e.g., for transferring holes from NGs into Gr), is expected to decrease with increasing NG sizes [see Fig. 1(b)]. For NG-sensitized oxide nanoparticles, the modification of interfacial energetics resulting from NG size variation has been shown to dominate the interfacial CT rate and efficiency.[23] Smaller NGs with higher interfacial energetics enable faster CT and thus higher CT quantum efficiency.[23] Furthermore, the reorganization energy, i.e., the energy required for charge solvation, and the resulting lattice distortions associated with CT may also affect CT in our system, given the molecular nature of NGs. Although the importance of vdW interactions in the NG–Gr vdWHs has been evidenced,[8] the interplay between the vdW interaction, interfacial energetics, and reorganization energy, and their impact on the CT processes, has remained elusive.

To address this question, herein we investigate photoinduced non-equilibrium CT dynamics in NG–Gr vdWHs with size-dependent interfacial interactions and energetics by varying the number of carbon atoms in the polyaromatic core from 42 to 96 [see Fig. 1(c)]. By employing optical-pump THz-probe (OPTP) spectroscopy, we demonstrate that the interfacial CT direction is universal in all the studied NG–Gr vdWHs with photogenerated holes transferring from NGs to Gr [as illustrated in Fig. 1(d)]. The resulting charge separation at NG–Gr interfaces is very long-lived (beyond 1 ns), leading to a photogating effect in Gr. More importantly, the interfacial CT efficiency in NG–Gr vdWHs is found to increase with NG sizes. By disentangling different contributions to the overall efficiency, we find that the electronic coupling at the NG–Gr interface dictated by the interlayer vdW interaction, rather

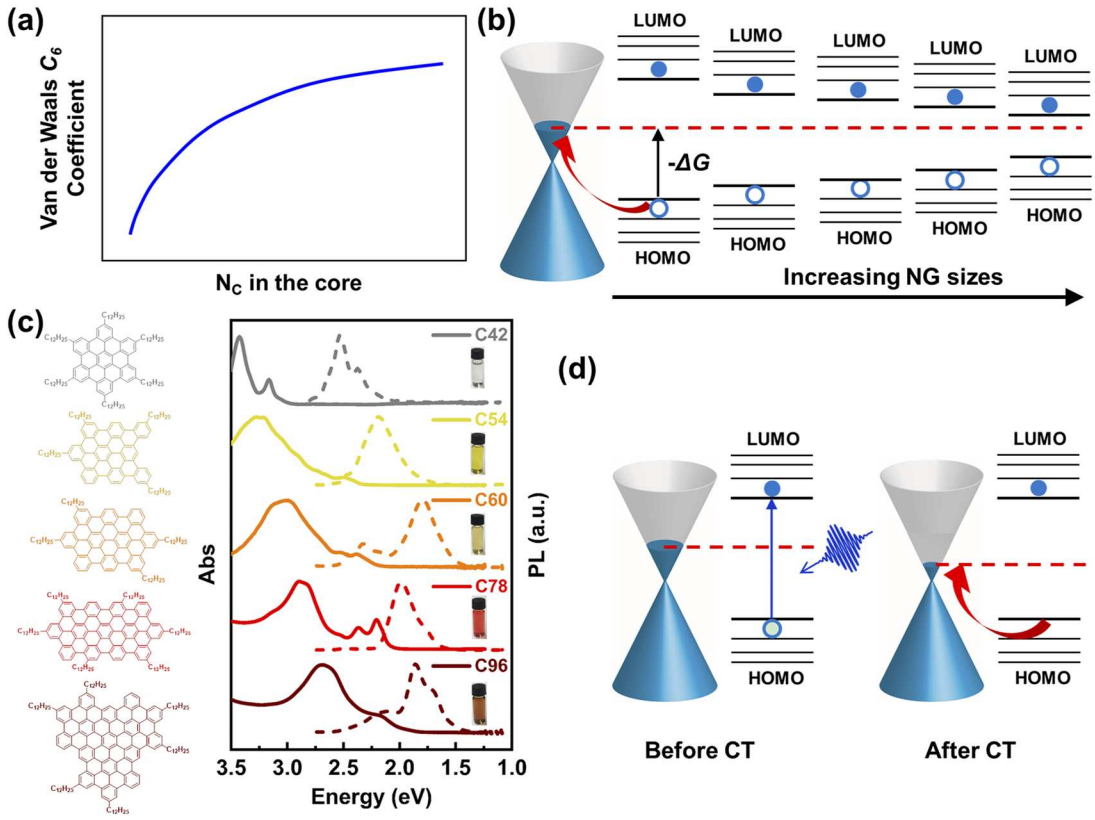

FIG. 1. Concept of monitoring and tuning interfacial CT in NG–Gr vdWHs. (a) Schematic of vdW interactions in NGs as a function of the number of carbon atoms in the polyaromatic core. As defined by the vdW C_6 coefficient, the vdW interaction in NG increases with the increasing number of carbon atoms in the polyaromatic core, following Refs. 21 and 22. (b) Schematic of the band alignment and photoinduced hole transfer process from NG to Gr. The driving force ($-\Delta G$) for photoinduced hole transfer, i.e., the energy difference between the highest occupied molecular orbital (HOMO) of NG and the Fermi energy level of Gr as depicted by the black arrow decreases with the increasing number of carbon atoms in the polyaromatic core. (c) Chemical structures, absorbance, and photoluminescence spectra of NGs used in this study; from top to bottom: C42, C54, C60, C78, and C96. (d) Schematic of the Fermi energy level modulation of Gr following the photoinduced hole transfer from NG to Gr.

© Author(s) 2022

than interfacial energetics or reorganization energy, plays the dominant role in determining the interfacial CT efficiency. Our results shed light on the CT mechanism in NG–Gr vdWHs and provide an effective knob to control the electronic coupling strength at NG–Gr interfaces by tuning the size-dependent vdW interactions.

II. EXPERIMENTAL SECTION

A. Sample preparation

The nanographene (NG) molecules used in this study were synthesized via a bottom-up approach, as reported in Refs. 24–27. We first dissolved NGs in powder form into toluene to get 1 mg/ml NG dispersions. Graphene (Gr) samples supported on 1 mm thick copper substrates were purchased from Grolltex, Inc. and grown by the chemical vapor deposition (CVD) method. We transferred Gr onto fused silica substrates for THz measurements following a wet transfer manner.[28,29] First, we spin-coated Gr samples with cellulose acetate butyrate (CAB) at 4000 rpm and baked them at 180 °C for 3 min. Then, the CAB-coated Gr samples were immersed into 1 M solution of ammonium persulfate (APS) for 10 min and rinsed with deionized (DI) water five times to remove Gr on the backside of copper substrates. The copper substrates were then fully etched by soaking the samples into 0.1 M APS solution for 2 h and rinsed with DI water five times to remove the attached ions. Afterward, Gr monolayers were "fished" onto the silica substrate, and CAB was removed by acetone (by 12 h soaking) and isopropanol (1 h) treatments. We prepared the NG–Gr van der Waals heterostructures (vdWHs) by spin-coating 20 μl NG dispersions on Gr samples three times in the glovebox and heating them at 100 °C for 10 min to remove residual toluene.

B. UV–visible absorption measurement

For the UV–vis absorption measurements of NG dispersions, 100 μl NG dispersions were diluted to 3 ml diluents and injected into cuvettes of 1 cm light path. The measurements were carried out on a Perkin–Elmer Lambda 900 spectrometer at room temperature. The spectrum was recorded with an interval of 2 nm. The UV–vis absorption measurements of NG films and NG–Gr vdWHs supported on the fused silica substrates were performed on a Perkin–Elmer 150 mm InGaAs Int. Sphere.

C. Optical pump-terahertz probe (OPTP) spectroscopy

THz measurements of Gr, NG, and NG–Gr vdWH samples were performed by an optical pump-terahertz probe (OPTP) setup. The fundamental laser output was generated by a regenerative Ti:sapphire amplifier system, which produces 4.5 mW, 50 fs pulses at a repetition rate of 1 kHz and a central wavelength of 800 nm. The generated pulses were then split into three branches for THz generation, sampling, and optical excitation. A single-cycle THz pulse of ~1 ps duration was generated by pumping a 1 mm thick (110) ZnTe crystal with the 800 nm fundamental pulses via optical rectification. We photoexcited samples to generate charge carriers using 400 nm pulses by frequency doubling the 800 nm fundamental pulses via a BaB_2O_4 (BBO) crystal. The time-dependent electrical field of the THz pulse was mapped out by the electro-optic sampling method.[30]

III. RESULTS AND DISCUSSION

Up to five NGs with an increasing number of carbon atoms in the polyaromatic core from 42 to 96 have been utilized to study the role of NG sizes on the interfacial CT process in NG–Gr vdWHs [see Fig. 1(c) for the structure; the alkyl chains at the peripheries are not considered for the nomenclature]. The right panel of Fig. 1(c) shows the UV–vis absorbance and PL spectra of NGs. As expected, the dominant absorption peaks gradually shift to a longer wavelength with the increasing lateral size of the NG. After NG deposition, Gr appears to be slightly n-doped with the Fermi level of ~0.2 eV above the Dirac point in C60-Gr vdWHs (see the associated discussion in the supplementary material).[8] The NG size is expected to only mildly affect the value of the Fermi level of Gr after deposition, given that the initial Fermi levels of NGs are similar and NGs are intrinsically undoped.

We examine the CT process in the heterostructure by employing ultrafast THz spectroscopy to track the photoconductivity dynamics in Gr following optical excitations to the vdWHs [see Fig. 2(a)]. In a typical OPTP measurement, we first excite the sample with 3.1 eV laser pulses (for a duration of ~100 fs) to generate charge carriers in the vdWHs. The photoconductivity is subsequently measured by a single-cycle THz pulse with ~1 ps duration (see details in Sec. II). Pure Gr shows a transient photoresponse on the order of a few ps due to the efficient charge carrier heating and cooling effects.[31,32] Conversely, in the vdWHs, interfacial CT could lead to a considerable change in the charge carrier density in Gr and, thus, a large conductivity modulation amplified by its high charge mobility. By knowing the initial Fermi level of Gr (~0.2 eV above the Dirac point) and CT-induced conductivity change, one could reliably identify both the direction and efficiency of interfacial CT in Gr-based vdWHs.[8,33,34]

As a control measurement, photoexcitation of pure Gr by 3.1 eV laser pulses results in a transient reduction in the conductivity with a lifetime of sub-10 ps [Fig. 2(b), red line]. The origin of such a "negative photoconductivity" has been well-understood and attributed to the enhanced momentum scattering of hot carriers in the photoexcited Gr with high charge carrier densities.[31,35–37] Following hot carrier cooling, the photoconductivity dynamics decays back to the equilibrium within several ps. We observe positive photoconductivity for pure NG films (using C96 film as an example). That is, the photo-injection of charge carriers into a semiconducting NG film leads to a transient increase in the conductivity [Fig. 2(b), brown line]. The magnitude of the positive THz photoconductivity of the NG film is substantially smaller than the negative THz photoconductivity of pure Gr, owing to the relatively low charge mobility of NG films. For the NG–Gr vdWHs, the same excitation density yields distinctly different photoconductivity from the individual Gr and NG films [Fig. 2(b), blue line]. Following the fast ~5 ps negative photoconductivity decay due to the hot carrier response in Gr, we observe a remarkably long-lived negative photoconductivity that persists well beyond 1 ns (limited by the range of our optical delay line). Given the initial Fermi level of Gr in the vdWH is ~0.2 eV above the Dirac point, the long-lived negative photoconductivity can be rationalized by a photoinduced hole injection process from NG to Gr (which is equivalent to transfer of "cold" electrons at the Fermi surfaces of graphene to NGs). This leads to a lowering of the Fermi level and thus electron density in Gr, decreasing the overall

© Author(s) 2022

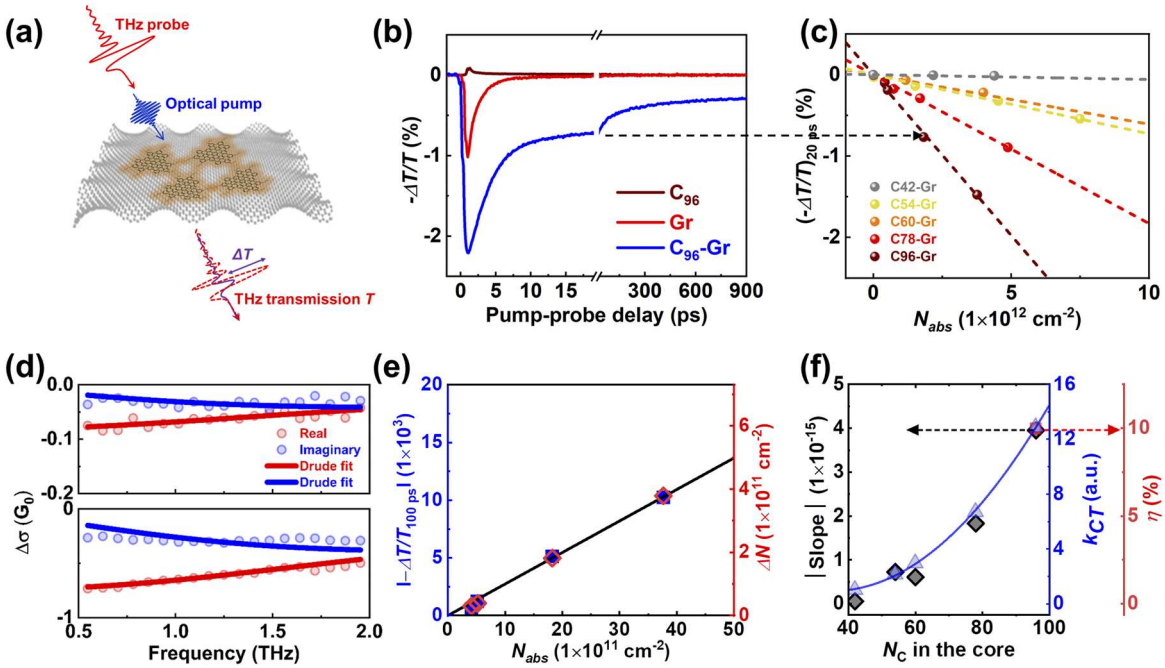

FIG. 2. Probing interfacial CT in NG–Gr vdWHs. (a) Illustration of monitoring interfacial charge transfer in NG–Gr vdWHs by OPTP spectroscopy. The heterostructure is photoexcited by a femtosecond pump pulse with a photon energy of 3.1 eV, above the bandgap of NGs (in blue), and the change in conductivity ($\Delta\sigma$) induced by the excitation is probed by a THz pulse (in red). The relative change in the THz transmission ($-\Delta T/T$) is linearly proportional to $\Delta\sigma$. (b) Time-resolved THz photoconductivity for C96 film (brown), Gr (red), and C96-Gr vdWH (blue). The samples are photoexcited by a femtosecond laser pulse with a photon energy of 3.1 eV (5.2 μJ/cm^2), after which the normalized THz transmission change $\Delta T/T$ is recorded under dry N_2 atmosphere. (c) $-\Delta T/T$ at a pump–probe delay of 20 ps for different NG–Gr vdWHs as a function of absorbed photon density. The dashed lines are the linear fits to the data. (d) Frequency-resolved complex THz photoconductivity for C96-Gr vdWHs at a pump–probe delay of ~100 ps with 1.5 (top) and 10.7 (bottom) μJ/cm^2 photoexcitation. The red and blue solid lines represent one Drude fit each to simultaneously the real and imaginary components of the complex THz photoconductivity. (e) Quantification of the photoinduced hole transfer efficiency for C96-Gr vdWH. The left y axis shows the absolute value of $-\Delta T/T$ at a pump–probe delay of 100 ps. The right y axis shows the density of transferred holes from NG to Gr inferred from the Drude model. (f) Photoinduced hole transfer efficiency for NG–Gr vdWHs as a function of the number of carbon atoms in the polyaromatic core. The left y axis shows the "relative" hole transfer efficiencies for different NG–Gr vdWHs by plotting the absolute values of the slopes of the linear fits as shown in Fig. 2(b), and the right red y axis shows the absolute charge transfer efficiencies by using the inferred efficiency at ~100 ps for C96-Gr vdWH as a reference. The blue data points on their own y axis represent the (relative) CT rate calculated from Marcus theory, as presented in the main text. The solid blue line represents a polynomial fitting to the blue data points.

conductivity. Such a hole transfer scenario is in line with our previous studies for WS_2-Gr and C60-Gr vdWHs by the above-bandgap excitations.[8,33] Here, we neglect the contribution of hot electron transfer (HET) from Gr to NG for the following reasons: First, the samples are pumped by 3.1 eV laser pulses where the Gr and NG layers are both photoexcited. However, the majority of charge carriers are populated mainly in the NG layer since the absorption of NG is much stronger compared to that of Gr (>17% in NG vs ~2% in Gr at 3.1 eV, Fig. S1). Thus, the contribution of hot carriers in Gr is expected to be limited. Second, the authors of Refs. 33 and 38 have shown that thermalized or non-thermalized hot electrons can be injected from Gr to WS_2 following subbandgap excitations. In the former case, following optical excitations, the photogenerated hot electrons can rapidly heat the charge carriers at the Fermi surface within tens of fs, generating thermalized hot carriers with a defined electron temperature obeying the Fermi–Dirac distribution. During the HET process, only hot electrons with sufficiently high energy can be emitted over the Schottky barrier into WS_2. In the latter case, injection of nascent non-thermalized electrons has also been suggested with quantum efficiency exceeding 50% when the interfacial electronic coupling is strong and the energetics of nascent hot carriers are higher than the Schottky barrier.[38] In our study, the nascent non-thermalized HET scenario can be ruled out because the energetics of nascent hot carriers in Gr following 3.1 eV excitations (~1.55 eV) is still below the required energy threshold for non-thermalized HET (over ~2 eV for C96). In addition, to test whether thermalized hot electrons in Gr contribute to CT, we have conducted control measurements by exciting only the Gr layer in the vdWHs with 1.55 eV excitations. Varied pump fluences are used to excite the system to increase the electron temperature in Gr and, thus, the probability of thermalized HET from Gr to NG (if there is any). As shown in Fig. S6, we observed no signature of CT from Gr to NGs with 1.55 eV excitations in the employed pump fluence range, ruling out the role of thermalized HET in CT. These control measurements strongly support our assignment of hole transfer from NGs to Gr as the main CT channel following optical excitations.

After confirming that the hole transfer mechanism prevails in the NG–Gr vdWHs, we further investigate the role of the NG size

© Author(s) 2022

in the CT efficiency. For a better comparison, we summarize the photoconductivity at ~20 ps for different NG–Gr vdWHs by varying the absorbed photon density (N_{abs}), as shown in Fig. 2(c). At the delay time of 20 ps, the hot carriers in graphene have relaxed back to the equilibrium. The remaining long-lived signal can be attributed to the photoconductivity changes due to CT. The photoconductivity at a fixed N_{abs} or the slope of the photoconductivity $-N_{abs}$ curve in Fig. 2(c), therefore, represents the relative interfacial hole transfer efficiency, as summarized in Fig. 2(f) (with the left y axis; see Fig. S5 for all raw dynamics). As we can see, the smallest NG used in this study, C42, shows essentially ~0% CT efficiency; the CT signal goes up with increasing NG sizes. At first glance, the observed trend in the size-dependent CT rate is surprising, given that the interfacial CT driving force (see Table S4), i.e., the energy difference between the ionization potential of NG and the chemical potential in Gr, is decreasing with an increase in the NG size. The obtained results seem to point to a dominant role of electronic coupling over interfacial energetics in determining the CT efficiencies in the NG–Gr vdWHs: for vdWHs consisting of small NGs, the interfacial vdW interactions are weak, as determined by its small size and low vdW interaction normalized by the number of sp^2 carbon atoms.[22] Our results indicate that this yields weak electronic coupling and thus negligible charge flow through the interfaces. By increasing the NG size, the vdW force increases drastically, enhancing the electronic coupling and favoring interfacial CT. To test this hypothesis, we provide further analysis by taking into account the contributions of the interfacial energetics, coupling strength, and reorganization energy to the overall CT rates.

In principle, the competition between interfacial CT (at a rate k_{CT}) and recombination (at a rate k_R) inside NGs dictates the hole transfer efficiency η from NGs to Gr, following $\eta = \frac{k_{CT}}{k_{CT}+k_R}$. The fact that only a small fraction of charge carriers (up to ~10% for C96; see the efficiency estimation in the following discussion) are transferred from NGs to Gr indicates the presence of ultrafast competition processes characterized by a rate k_R, with $k_{CT} \ll k_R$. As such, η can be approximated by $\eta \sim \frac{k_{CT}}{k_R}$. The detailed recombination/loss channels remain elusive, which calls for further investigation.

To rationalize our observation of the enhanced hole transfer efficiency η with increasing NG size, we apply Marcus theory to account for the relative contributions of the coupling strength V, driving force $-\Delta G$, and reorganization energy λ to the overall k_{CT}. The rate of hole transfer from the HOMO level in NGs to the continuum accepting states in Gr reads[23,39,40]

$$k_{CT} = \frac{2\pi}{\hbar\sqrt{4\pi k_B T}} V^2 g(\lambda, \Delta G), \tag{1}$$

$$\text{with } g(\lambda, \Delta G) = \frac{1}{\sqrt{\lambda}} \int_0^{-\Delta G} dE f(E + \Delta G + \mu) v(E + \Delta G + \mu) \times \exp\left(-\frac{(\lambda + E + \Delta G)^2}{4\lambda k_B T}\right), \tag{2}$$

where the zero-energy reference is the ionization potential of NG (see Table S3). The driving force for CT, $-\Delta G$, is the energy difference between the ionization potential of NG and the chemical potential μ in Gr. $\hbar$ is the reduced Planck constant, k_B is the Boltzmann constant, and T is the temperature. $v(|E + \Delta G + \mu|) = \frac{2|E+\Delta G+\mu|}{\pi(\hbar v_F)^2}$ is the density of states of Gr around the Dirac point, and $f(|E + \Delta G + \mu|) = \frac{1}{e^{(|E+\Delta G+\mu|-\mu)/k_B T}+1}$ is the Fermi–Dirac distribution. The reorganization energy is calculated using density functional theory at the PBE0-D3(BJ)/def2-TZVP//PBE0-D3(BJ)/def2-SVP level of theory[41–45] (see Table S2 and Sec. 3 in the supplementary material for computational details). The electronic coupling strength V depends on the donor–acceptor wave function overlap and, therefore, the distance between NG and Gr, determined by the vdW attraction strength between NG and Gr (given by the C_6 coefficient of NGs[22]). We assume that V is linearly proportional to the interfacial vdW attraction strength as a first-order approximation. Integrating Eq. (1), we find that the estimated k_{CT} trend with NG size matches well to the relative hole transfer efficiency, as shown in Fig. 2(f) (the right blue axis). This result indicates that the variation of k_R is substantially smaller than that of k_{CT} in our experimental systems, when increasing NG size.

Moreover, our estimation disentangles the relative weight of each contribution to the CT: by increasing the size of NG from C42 to C96, the contribution of the coupling term increases by an order of magnitude, thus dictating the overall size-dependent k_{CT}. k_{CT} is not sensitive to changes in $-\Delta G$ since its variation over hundreds of meV shows a negligible impact on k_{CT}. This is not surprising, given that $-\Delta G$ is substantially larger than λ, so that the transfer of holes from the HOMO of NGs to each individual accepting state (with $-\Delta G > \lambda$) lies in the Marcus inverted region, with k_{CT} rapidly decreasing with increasing $-\Delta G$. In addition, λ plays a minor role, resulting in a small enhancement factor of 1.2 for the largest NG used in this study. Overall, the electronic coupling strength seems to be the primary factor affecting the efficiency of hole injection from NGs to Gr. We note that the previous study on CT between NG and a metal oxide revealed a dominant role of ΔG in determining NG-size-dependent CT rates.[23] In that NG-sensitized oxide system, interfacial coupling is expected to be weak and invariant with NG sizes. In line with our recent report on the uniqueness of the NG–Gr systems:[8] thanks to the strong π–π interaction at their interfaces, our results here indicate that the electronic coupling strength plays a paramount role in determining CT rates in the constituted all-carbon-based vdW heterostructures.

Finally, to demonstrate the relevance of the heterostructure for applications, we independently determine the absolute CT efficiency η, which is defined as $\eta = \frac{N_{CT}}{N}$. Here, N_{CT} represents the number of transferred holes and N is the number of photogenerated charge carriers, which equates to the product of the number of photons absorbed in the NG layer (N_{abs}) and the photon-to-charge conversion efficiency (φ). To quantify N_{CT}, we employ THz time-domain spectroscopy (THz-TDS) to measure the complex photoconductivity of C96-Gr vdWHs at ~100 ps, where the contributions from the hot carrier effect in Gr and excitons in C96 to the complex photoconductivity are expected to be null. In the THz-TDS measurements, we map out the entire THz waveforms without (as a reference) and with photoexcitations at a certain pump–probe delay. We can then convert the pump-induced THz absorption and phase shift in the time domain into the complex photoconductivity spectra in the frequency domain (see details in the supplementary material, Sec. 2). Figure 2(d) shows two exemplary complex photoconductivities at different pump fluences. The obtained photoconductivity can be described by the conductivity difference between the quasi-equilibrium states in Gr before and after hole

© Author(s) 2022

injection. Both the states can be well-described by the Drude model. This analysis provides the charge carrier density and scattering time in Gr following hole injection (see details in the supplementary material, Sec. 2). Knowing the N_{CT} (from THz-TDS) and N_{abs} (from absorption), we can estimate the CT quantum yield η ($=N_{CT}/N \sim N_{CT}/N_{abs}$) to be ~10% at 100 ps for C96-Gr vdWHs. Note that the actual total η following hole transfer (taking place at sub-10 ps) is underestimated, given that the photon-to-charge conversion efficiency of C96 here is assumed to be 100% (i.e., $N = N_{abs}$) and partial back recombination has taken place within 100 ps (see details in the supplementary material).

IV. CONCLUSION

In summary, we elucidated the origin of the interfacial CT in NG–Gr vdWHs by systematically varying the NG sizes to tune the interlayer vdW interactions. We found that vdW interactions play a dominant role in determining the interfacial CT efficiency, whereas interfacial energetics and reorganization energy have a minor influence. By increasing the size of NGs from 42 to 96 carbon atoms in the polyaromatic core to enhance the interfacial coupling strength, we find that the CT efficiency increases by one order of magnitude, despite the interfacial energy driving the CT process being unfavorably reduced. Our results provide critical insights into the CT mechanism and offer a new tool to tune the electronic coupling at NG–Gr interfaces by controlling the size-dependent vdW interactions.

SUPPLEMENTARY MATERIAL

See the supplementary material for measurement details and computational methods.

ACKNOWLEDGMENTS

X.Y. and S.F. thank the fellowship support from the China Scholarship Council (CSC). M.M. acknowledges the postdoctoral support from the Alexander von Humboldt Foundation. Research in Strasbourg has been supported by the European Commission through the ERC project SUPRA2DMAT (Grant No. GA-833707), the Graphene Flagship Core 3 project (Grant No. GA-881603), the Agence Nationale de la Recherche through the Labex project CSC (Grant No. ANR-10-LABX-0026 CSC) within the Investissement d'Avenir program (Grant No. ANR-10-120 IDEX-0002-02), the International Center for Frontier Research in Chemistry (icFRC), and the Institut Universitaire de France (IUF). We acknowledge funding support from the Max Planck Society.

AUTHOR DECLARATIONS

Conflict of Interest

The authors declare no conflicts of interest.

Author Contributions

X.Y. and S.F. contributed equally to this work.

DATA AVAILABILITY

The data that support the findings of this study are available from the corresponding author upon reasonable request.

REFERENCES

[1] A. Narita, X.-Y. Wang, X. Feng, and K. Müllen, Chem. Soc. Rev. **44**, 6616 (2015).
[2] X. Yao, X.-Y. Wang, C. Simpson, G. M. Paternò, M. Guizzardi, M. Wagner, G. Cerullo, F. Scotognella, M. D. Watson, A. Narita, and K. Müllen, J. Am. Chem. Soc. **141**, 4230 (2019).
[3] B. V. Senkovskiy, M. Pfeiffer, S. K. Alavi, A. Bliesener, J. Zhu, S. Michel, A. V. Fedorov, R. German, D. Hertel, D. Haberer, L. Petaccia, F. R. Fischer, K. Meerholz, P. H. M. van Loosdrecht, K. Lindfors, and A. Grüneis, Nano Lett. **17**, 4029 (2017).
[4] S. K. Alavi, B. V. Senkovskiy, M. Pfeiffer, D. Haberer, F. R. Fischer, A. Grüneis, and K. Lindfors, 2D Mater. **6**, 035009 (2019).
[5] Y.-C. Chen, D. G. de Oteyza, Z. Pedramrazi, C. Chen, F. R. Fischer, and M. F. Crommie, ACS Nano **7**, 6123 (2013).
[6] V. Bonal, R. Muñoz-Mármol, F. Gordillo Gámez, M. Morales-Vidal, J. M. Villalvilla, P. G. Boj, J. A. Quintana, Y. Gu, J. Wu, J. Casado, and M. A. Díaz-García, Nat. Commun. **10**, 3327 (2019).
[7] Y. Yan, D. Zhai, Y. Liu, J. Gong, J. Chen, P. Zan, Z. Zeng, S. Li, W. Huang, and P. Chen, ACS Nano **14**, 1185 (2020).
[8] Z. Liu, H. Qiu, S. Fu, C. Wang, X. Yao, A. G. Dixon, S. Campidelli, E. Pavlica, G. Bratina, S. Zhao, L. Rondin, J.-S. Lauret, A. Narita, M. Bonn, K. Müllen, A. Ciesielski, H. I. Wang, and P. Samorì, J. Am. Chem. Soc. **143**, 17109 (2021).
[9] P. Fantuzzi, A. Candini, Q. Chen, X. Yao, T. Dumslaff, N. Mishra, C. Coletti, K. Müllen, A. Narita, and M. Affronte, J. Phys. Chem. C **123**, 26490 (2019).
[10] G. Konstantatos, M. Badioli, L. Gaudreau, J. Osmond, M. Bernechea, F. P. G. de Arquer, F. Gatti, and F. H. L. Koppens, Nat. Nanotechnol. **7**, 363 (2012).
[11] D. De Fazio, B. Uzlu, I. Torre, C. Monasterio-Balcells, S. Gupta, T. Khodkov, Y. Bi, Z. Wang, M. Otto, M. C. Lemme, S. Goossens, D. Neumaier, and F. H. L. Koppens, ACS Nano **14**, 11897 (2020).
[12] F. H. L. Koppens, T. Mueller, P. Avouris, A. C. Ferrari, M. S. Vitiello, and M. Polini, Nat. Nanotechnol. **9**, 780 (2014).
[13] K. Roy, M. Padmanabhan, S. Goswami, T. P. Sai, G. Ramalingam, S. Raghavan, and A. Ghosh, Nat. Nanotechnol. **8**, 826 (2013).
[14] J. D. Mehew, S. Unal, E. Torres Alonso, G. F. Jones, S. Fadhil Ramadhan, M. F. Craciun, and S. Russo, Adv. Mater. **29**, 1700222 (2017).
[15] F. Schulz, P. H. Jacobse, F. F. Canova, J. Van Der Lit, D. Z. Gao, A. Van Den Hoogenband, P. Han, R. J. M. Klein Gebbink, M.-E. Moret, P. M. Joensuu, I. Swart, and P. Liljeroth, J. Phys. Chem. C **121**, 2896 (2017).
[16] T. Wassmann, A. P. Seitsonen, A. M. Saitta, M. Lazzeri, and F. Mauri, J. Am. Chem. Soc. **132**, 3440 (2010).
[17] X. Yao, W. Zheng, S. Osella, Z. Qiu, S. Fu, D. Schollmeyer, B. Müller, D. Beljonne, M. Bonn, H. I. Wang, K. Müllen, and A. Narita, J. Am. Chem. Soc. **143**, 5654 (2021).
[18] L. Chen, Y. Hernandez, X. Feng, and K. Müllen, Angew. Chem., Int. Ed. **51**, 7640 (2012).
[19] O. Gröning, S. Wang, X. Yao, C. A. Pignedoli, G. B. Barin, C. Daniels, A. Cupo, V. Meunier, X. Feng, A. Narita, K. Müllen, P. Ruffieux, and R. Fasel, Nature **560**, 209 (2018).
[20] Y.-W. Son, M. L. Cohen, and S. G. Louie, Phys. Rev. Lett. **97**, 216803 (2006).
[21] J. Björk, F. Hanke, C. A. Palma, P. Samori, M. Cecchini, and M. Persson, J. Phys. Chem. Lett. **1**, 3407 (2010).
[22] V. V. Gobre and A. Tkatchenko, Nat. Commun. **4**, 2341 (2013).
[23] P. Han, X. Yao, K. Müllen, A. Narita, M. Bonn, and E. Cánovas, Nanoscale **12**, 16046 (2020).
[24] T. Böhme, C. D. Simpson, K. Müllen, and J. P. Rabe, Chem. - Eur. J. **13**, 7349 (2007).
[25] X. Yang, X. Dou, A. Rouhanipour, L. Zhi, H. J. Räder, and K. Müllen, J. Am. Chem. Soc. **130**, 4216 (2008).
[26] D. Wasserfallen, M. Kastler, W. Pisula, W. A. Hofer, Y. Fogel, Z. Wang, and K. Müllen, J. Am. Chem. Soc. **128**, 1334 (2006).

© Author(s) 2022

[27] Ž. Tomović, M. D. Watson, and K. Müllen, Angew. Chem., Int. Ed. **43**, 755 (2004).
[28] N. Yogeswaran, W. T. Navaraj, S. Gupta, F. Liu, V. Vinciguerra, L. Lorenzelli, and R. Dahiya, Appl. Phys. Lett. **113**, 014102 (2018).
[29] G. Burwell, N. Smith, and O. Guy, Microelectron. Eng. **146**, 81 (2015).
[30] R. Ulbricht, E. Hendry, J. Shan, T. F. Heinz, and M. Bonn, Rev. Mod. Phys. **83**, 543 (2011).
[31] G. Jnawali, Y. Rao, H. Yan, and T. F. Heinz, Nano Lett. **13**, 524 (2013).
[32] K. J. Tielrooij, J. C. W. Song, S. A. Jensen, A. Centeno, A. Pesquera, A. Zurutuza Elorza, M. Bonn, L. S. Levitov, and F. H. L. Koppens, Nat. Phys. **9**, 248 (2013).
[33] S. Fu, I. du Fossé, X. Jia, J. Xu, X. Yu, H. Zhang, W. Zheng, S. Krasel, Z. Chen, Z. M. Wang, K. J. Tielrooij, M. Bonn, A. J. Houtepen, and H. I. Wang, Sci. Adv. **7**, eabd9061 (2021).
[34] G. Jnawali, Y. Rao, J. H. Beck, N. Petrone, I. Kymissis, J. Hone, and T. F. Heinz, ACS Nano **9**, 7175 (2015).
[35] S.-F. Shi, T.-T. Tang, B. Zeng, L. Ju, Q. Zhou, A. Zettl, and F. Wang, Nano Lett. **14**, 1578 (2014).
[36] A. J. Frenzel, C. H. Lui, Y. C. Shin, J. Kong, and N. Gedik, Phys. Rev. Lett. **113**, 056602 (2014).
[37] S. A. Jensen, Z. Mics, I. Ivanov, H. S. Varol, D. Turchinovich, F. H. L. Koppens, M. Bonn, and K. J. Tielrooij, Nano Lett. **14**, 5839 (2014).
[38] Y. Chen, Y. Li, Y. Zhao, H. Zhou, and H. Zhu, Sci. Adv. **5**, eaax9958 (2019).
[39] R. A. Marcus, Annu. Rev. Phys. Chem. **15**, 155 (1964).
[40] R. A. Marcus and N. Sutin, Biochim. Biophys. Acta, Rev. Bioenerg. **811**, 265 (1985).
[41] C. Adamo and V. Barone, J. Chem. Phys. **110**, 6158 (1999).
[42] F. Weigend and R. Ahlrichs, Phys. Chem. Chem. Phys. **7**, 3297 (2005).
[43] F. Weigend, Phys. Chem. Chem. Phys. **8**, 1057 (2006).
[44] S. Grimme, J. Antony, S. Ehrlich, and H. Krieg, J. Chem. Phys. **132**, 154104 (2010).
[45] S. Grimme, S. Ehrlich, and L. Goerigk, J. Comput. Chem. **32**, 1456 (2011).

© Author(s) 2022